Optimal Vehicle Following Strategy for Joint Velocity and Energy Management Control of Series Hybrid Electric Vehicles

Xiao Pan [*] Boli Chen [**] Simos A. Evangelou [***]

[*] Department of Electrical and Electronic Engineering, Imperial College London, UK, (e-mail: xiao.pan17@imperial.ac.uk).
[**] Department of Electronic and Electrical Engineering, University College London, UK, (e-mail: boli.chen@ucl.ac.uk)
[***] Department of Electrical and Electronic Engineering, Imperial College London, UK, (e-mail: s.evangelou@imperial.ac.uk)

Abstract: Recent advances in information and communication technologies present opportunities to optimally control the driving speed and powertrain energy management of vehicles under dynamic traffic circumstances. This paper addresses the energy-efficient car following problem of a series hybrid electric vehicle (HEV) by an enhanced adaptive cruise control (EACC) method. EACC is based on a nonlinear model predictive control framework, in which the behaviour of the lead vehicle is forecast by a neural network predictor trained by common test cycles. With the real-time predicted reference speed, EACC simultaneously optimizes the velocity and energy source power split of the ego HEV, while keeping the inter-vehicular distance within the desired range. The performance of EACC is benchmarked against a practical adaptive cruise control (ACC) that performs drafting and an impractical optimal control (OC) solved throughout the entire journey. Numerical examples show that the EACC can effectively close the gap between ACC and OC in terms of optimality with a remarkable fuel saving over ACC, while the computational load of EACC is comparable to ACC, which is much more efficient than the OC. Further design insight of the methodology is also provided by an investigation into the influence of the prediction horizon.

Keywords: Hybrid Electric Vehicle, Optimal Control, Energy Management, Velocity Control, Model Predictive Control.

As a result of multiple energy sources, hybrid electric vehicles (HEVs) can profit from freely optimized power split between the energy sources for improving fuel economy as compared to the conventional vehicles. The problem of finding fuel-efficient power split for HEVs, which is referred to as energy management (EM) control problem, has drawn considerable attention in the past decade. A comprehensive overview of existing EM techniques, from rule-based to optimization-based, can be found in (Martinez et al., 2017). In particular, optimization-based EM strategies are popular as benchmark methods due to usually guaranteeing the optimal or sub-optimal solutions (Li et al., 2017b; Uebel et al., 2019).

Recently, with the advent of the advanced vehicle-to-vehicle (V2V) and vehicle-to-infrastructure (V2X) communication technologies, the interconnected vehicle control is gaining momentum (Chen and Evangelou, 2019; Malikopoulos et al., 2018; Martinez et al., 2017). This leads to the investigation of a new optimisation framework that considers the EM for connected HEVs (Li et al., 2017a; Xie et al., 2019; Zhang et al., 2019), such as vehicle platooning with a fleet of HEVs, or with only two vehicles (car following model), which is a natural way to emulate real-world driving conditions. In this context, both the driving speed and EM are possible to be optimized to improve overall efficiency and to cut emissions, while maintaining or even improving the traffic throughput. Moreover, the availability of the various communication systems enables the prediction of the driving speed of the leading vehicle based on the traffic conditions. Thus, the investigation of predictive EM optimization for real-time implementation is gaining momentum (Liu et al., 2017; Murphey et al.,

2013; Zou et al., 2016). The fundamental challenge in the design of predictive EM control techniques is associated with the precision of velocity prediction. Various speed prediction methods are compared in (Sun et al., 2014) in the context of HEVs. It is shown that the neural network (NN) predictor tends to achieve the best performance as compared to the approaches based on exponentially varying speed predictors and Markov chain.

This paper proposes an enhanced adaptive cruise control (EACC) to address the car following problem, where the speed and EM of the ego vehicle are optimally controlled with consideration of the interaction with the vehicle ahead. Compared to the very recent work on the car following EM (Xie et al., 2019), the presented paper addresses a more realistic car following scenario, where the influence of following distance on the air drag losses is modelled. As such, the ego vehicle can make use of drafting technique to reduce aerodynamic energy losses. Moreover, the vehicle jerk is modeled to ensure smooth control, and therefore it improves driving comfort and avoids unrealistic jerky manoeuvre. The focus of the paper is on the series HEV powertrain architecture. However, the ideas that are presented also have relevance to other HEV architectures. The fundamental concept of EACC is the nonlinear model predictive control (NMPC), which optimizes the velocity and power split over a sliding time window based on the predicted reference speed of the lead vehicle. In this work, the reference speed is forecast by the NN predictor introduced in (Sun et al., 2014). The performance of the proposed EACC is evaluated by comparing it with two benchmark methods: 1) the optimal control (OC) solution solved globally with a precise speed profile of the lead vehicle, and 2) a practical adaptive

cruise control (ACC) method that is also based on NMPC, whereas a constant and close following distance is targeted to enjoy the drafting effect. Additionally, the impact of the prediction horizon length on the overall optimality is investigated.

This paper is organized as follows. Section 1 introduces the car following scheme and the powertrain model of the series HEV. The proposed method is described in Section 2, together with two benchmark methods. Simulation examples and comparative studies are illustrated in Section 3, followed by the concluding remarks in Section 4.

1. MODEL DESCRIPTION

1.1 Vehicle following Model

This work considers the car following model illustrated in Fig. 1, where the vehicle in front is identified as an uncontrolled reference vehicle, followed by a controlled ego vehicle. Moreover, it is assumed that the lead vehicle is travelling at a speed v_{ref}, and the past status of the lead vehicle, including the speed and travelled space, (v_{ref}, s_{ref}) can be shared with the ego vehicle by proper communication systems without any delay.
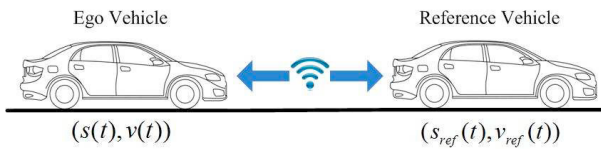

Fig. 1. Vehicle following scheme with V2V communication considered.

Consider (s, v) respectively the distance and speed of the ego vehicle. The inter-vehicular distance, d, between the two vehicles is defined by $d \triangleq s_{ref} - s$. To keep following the vehicle in front safely, the gap between the two vehicles is constrained by:

$$d_{\min} \leq d \leq d_{\max}, \qquad (1)$$

where $d_{\min}$ is the minimum distance to avoid rear-end collision and $d_{\max}$ is the maximum value to maintain the car following mode. The selections of $d_{\min}$ and $d_{\max}$ depend on the road type and vehicle travelling speed.

The ego vehicle motion is given in terms of speed and travelled space by the following differential equations:

$$\frac{d}{dt}s = v, \qquad (2a)$$

$$m\frac{d}{dt}v = F_w + F_h - f_T\, m\, g - f_D(d)\, v^2, \qquad (2b)$$

where $m = 1500\,\mathrm{kg}$ is the vehicle mass, F_w is the powertrain driving force at the wheels, F_h is the braking force, $f_T = 0.01$, is the coefficient of tyre rolling resistance, and $f_D(d)$ is the aerodynamic drag coefficient, modelled as a function of the distance to the lead vehicle (Rodrigues Lopes and Evangelou, 2019; Turri et al., 2017).

For an HEV with energy recovery system, $F_w > 0$ in driving condition (energy transfer from the powertrain to the vehicle) and $F_w \leq 0$ during energy recovery. As commonly assumed in EM studies (Uebel et al., 2019), the regenerative braking is assumed not restricted by the braking distribution between front and rear axles, such that all the braking power is recoverable and it is only restricted by the battery power charging limit.

The present work adopts the nonlinear air drag model (Rodrigues Lopes and Evangelou, 2019) that is able to capture the influence of inter-vehicular distance on the

drag coefficient in the context of a passenger car. The behaviour of the model is illustrated in Fig. 2. As it can
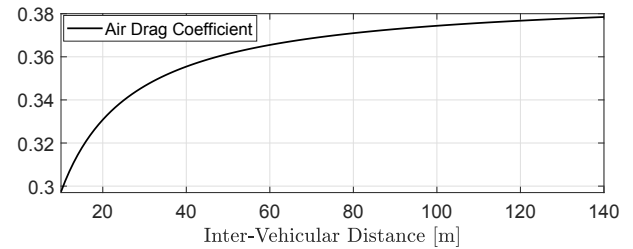

Fig. 2. Air drag coefficient of a passenger car, modeled as a function of inter-vehicular distance (Rodrigues Lopes and Evangelou, 2019).

be seen, the air drag coefficient, and consequently the aerodynamic losses can be effectively reduced by travelling close to the reference vehicle because of the drafting effect.

1.2 Series Hybrid Electric Vehicle Powertrain Model

The series HEV powertrain architecture is sketched in Fig. 3. As it can be seen, a series HEV consists of two en-
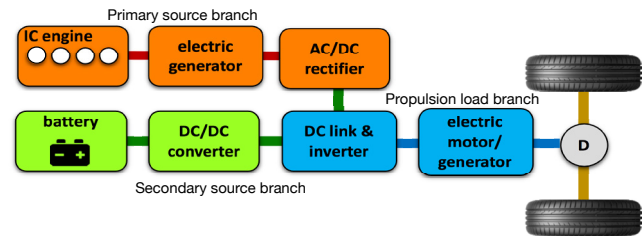

Fig. 3. Block diagram of the series HEV powertrain.

ergy source branches: the primary source branch (PS) and the secondary source branch (SS), which are joined electrically at the DC-link. Then, the total power is delivered to the driving wheels via the traction electric motor. Mechanical brakes may be actuated to decelerate the vehicle. Energy regeneration is also possible during decelerations conveying braking power through the transmission up to the battery. Moreover, the SS may be recharged by using a fraction of the PS power.

The vehicle model for the HEV is now briefly described. It represents a simple (i.e., quasi-steady) but representative model for HEV analysis and control design (Chen et al., 2019, 2018; Lujan et al., 2018; Zhou et al., 2015).

Primary Source Branch As shown in Fig. 3, the PS branch consists of a generator set and an AC-DC rectifier, which are connected in series. The mechanical separation of the PS from driving wheels allows the PS to be operated along its optimal efficiency trajectory. In this context, the fuel mass rate of the PS can be approximated as a linear function of PS output power, P_{PS}:

$$\frac{d}{dt}m_f = m_{f0} + \alpha_f P_{PS}, \qquad (3)$$

in which $m_{f0} = 0.061\,\mathrm{g/s}$ acts as the idling fuel mass rate, and $\alpha_f = 0.059\,\mathrm{g/kW/s}$ is the coefficient of power transformation. The two constants, in this paper, are obtained by linear regression fitting to the static PS efficiency map given in (Chen et al., 2019).

Secondary Source Branch The SS branch is composed of a battery and a DC-DC converter. In particular, the battery is modeled as series connection of an ideal voltage source with a resistance, and the dynamics are described as a pure integrator of SoC. Such a model has been

extensively used in the HEV EM literature (Chen et al., 2019; Zhou et al., 2015). The DC-DC converter is modelled as a constant efficiency term, $\eta_{dc} = 0.96$.

With the considerations above, the battery dynamics (i.e., SoC) are governed by:

$$\frac{d}{dt}\text{SoC} = \frac{-V_{oc} + \sqrt{V_{oc}^2 - 4P_{SS}\,R_b/\eta_{dc}^{\text{sign}(P_{SS})}}}{2R_b\,Q_{\max}}, \quad (4)$$

where P_{SS} is the branch output power with an assumed positive sign in the discharging phase, $V_{oc} = 300\,\text{V}$ is the constant open circuit voltage, $Q_{\max} = 5\,\text{Ah}$ is the battery capacity and $R_b = 0.2056\,\Omega$ is the internal resistance.

Propulsion Load Branch From the power flow within the PL branch, the powertrain driving force is determined by:

$$F_w = \frac{(P_{PS} + P_{SS})(\eta_i\eta_m\eta_t)^{\text{sign}(F_w)}}{v}, \quad (5)$$

where $\eta_i = 0.96$ and $\eta_t = 0.96$ are constant efficiencies of the inverter and the transmission, respectively. η_m is the efficiency of the bidirectional motor/generator, represented by an efficiency map as shown in the authors' previous work (Chen et al., 2019). The transmission system connects the motor/generator and wheels with a fixed gear ratio $g_t = 10$, such that $\omega_m = g_t v$.

Overall Vehicle Model In view of the vehicle model presented previously, the series HEV has three independent sources of power P_{SS}, P_{PS} and P_h, which are freely controlled to obtain the desired values of vehicle speed and acceleration. To ensure the smoothness of the control, the power variables are not controlled directly, instead, the control inputs in this work are the jerk variables, j_{PS}, j_{SS}, j_h of the associated forces, $F_{PS} = P_{PS}/v$, $F_{SS} = P_{SS}/v$, and $F_h = P_h/v$. Let us define the state variables $\boldsymbol{x} \triangleq [m_f, \text{SoC}, v, s, F_{PS}, F_{SS}, F_h]^\top$ and control inputs $\boldsymbol{u} \triangleq [j_{PS}, j_{SS}, j_h]$. Then, the overall vehicle model, $\frac{d}{dt}\mathbf{x} = \mathbf{f}(\mathbf{x}, \mathbf{u}, t)$ that collects (2), (3), (4) and the dynamics of the forces, is expressed as:

$$\frac{d}{dt}\begin{pmatrix} m_f \\ \text{SoC} \\ v \\ s \\ F_{PS} \\ F_{SS} \\ F_h \end{pmatrix} = \begin{pmatrix} q_{f0} + \alpha_f(P_{PL} - P_{SS}) \\ \dfrac{-V_{oc} + \sqrt{V_{oc}^2 - 4P_{SS}\,R_b/\eta_{dc}^{\text{sign}(P_{SS})}}}{2R_b\,Q_{\max}} \\ \dfrac{1}{m}\left(F_w + F_h - f_T\,m\,g - f_D(d)\,v^2\right) \\ v \\ mj_{PS} \\ mj_{SS} \\ mj_h \end{pmatrix} \tag{6}$$

Furthermore, following inequality constraints are also imposed due to physical and operational limits:

$$0 \le P_{PS} \le P_{PS_{\max}}, \quad P_{SS_{\min}} \le P_{SS} \le P_{SS_{\max}}, \tag{7a}$$

$$\text{SoC}_{\min} \le \text{SoC} \le \text{SoC}_{\max}, \quad 0 \le v \le v_{\max}, \tag{7b}$$

$$P_h \le 0, \quad j_{PS}, j_{SS}, j_h \in [j_{\min}, j_{\max}] \tag{7c}$$

with $P_{PS_{\max}} = 70\,\text{kW}$, $P_{SS_{\max}} = 30\,\text{kW}$, $P_{SS_{\min}} = -15\,\text{kW}$, $\text{SoC}_{\max} = 0.8$, $\text{SoC}_{\min} = 0.5$, which are chosen to emulate the energy sources for a non-plug-in HEV.

2. PROBLEM FORMULATION AND CAR FOLLOWING STRATEGIES

The main objective is to optimize the speed and EM of the ego vehicle over a specified time-horizon $[0, T]$, such that its fuel consumption $m_f(T)$ is minimized and the battery is charge sustained at the end of the mission (i.e., $\text{SoC}(0) \approx$

$\text{SoC}(T)$), subject to state and control constraints as well as the constraint on the inter-vehicular distance. To address the optimization problem online, this section proposes the EACC which combines receding horizon control with an NN-based speed predictor. Prior to the introduction of the novel scheme, benchmark strategies are introduced next.

2.1 Optimal Control (OC) Method

By assuming that the reference speed profile v_{ref} is available for all $t \in [0, T]$, it is immediate to obtain s_{ref} by integration with $s_{ref}(0) = d_0$, where d_0 is the initial distance between the two vehicles. Then the control problem can be formulated as an optimal control problem. The objective function is designed as:

$$J_{oc} = W_1 m_f(T) + W_2\left(\text{SoC}(T) - \text{SoC}(0)\right)^2 \tag{8}$$

where W_1, W_2 are two constant weights, tuned to balance the control performance in both aspects. The objective J_{oc} is minimized subject to system differential equations (6) and the inequality constraints (1) and (7). Finally, the problem is completed by imposing following boundary conditions: $s(0) = s_{ref}(0) - d_0 = 0$, $s(T) = s_{ref}(T) - d_0$, $v(0) = v_{ref}(0)$, $v(T) = v_{ref}(T)$, $F_{PS}(0) = F_{SS}(0) = F_h(0) = 0$, $m_f(0) = 0$, $\text{SoC}(0) = 0.65$, $\text{SoC}(t_0) = 0.65$, where SoC is initialized at the middle of the allowed SoC range, and the control forces and other states are initialized at 0. Furthermore, the terminal condition on s ensures the space travelled by the ego vehicle is identical to that travelled by the reference vehicle.

2.2 Adaptive Cruise Control (ACC) Strategy

During real-world driving, v_{ref} is usually not known a priori. This promotes the development of ACC strategies for driver assistance. Similarly to most of the available ACC systems (Shakouri and Ordys, 2014), the benchmark ACC considered in this paper aims to maintain a fixed distance from the vehicle ahead by adaptively adjusting the velocity of the ego vehicle. Additionally, to further improve the fuel efficiency of the ACC, and consequently to enable effective comparison with the proposed approach, it is also assumed that the benchmark ACC enforces the ego vehicle to stay closely behind the lead vehicle so that it can benefit from drafting. The ACC is designed based on an NMPC framework, in discrete time with sampling time T_s, formulated as follows:

$$\min_{\boldsymbol{u}} J_{k,\text{ACC}}, \ k = 1, 2, \ldots, T/T_s \tag{9a}$$

$$\textbf{s.t.:} \quad \boldsymbol{x}(t_{j+1}|t_k) = \mathbf{f}(\boldsymbol{x}(t_j|t_k), \boldsymbol{u}(t_j|t_k)), \ j = 1, \ldots, N_p, \tag{9b}$$

$$\boldsymbol{x}(t_k) = \boldsymbol{x_0}, \tag{9c}$$

$$\boldsymbol{\Psi}(\boldsymbol{x}(t_j|t_k), \boldsymbol{u}(t_j|t_k), \hat{\boldsymbol{x}}_r(t_j|t_k)) < 0, \ j = 1, \ldots, N_p, \tag{9d}$$

where N_p is the dimension of the prediction horizon, and $\hat{\boldsymbol{x}}_r \triangleq [\hat{v}_{ref}, \hat{s}_{ref}]$ represents the predicted reference velocity and space. The ACC assumes that the reference vehicle keeps its speed constant within a prediction horizon:

$$\hat{v}_{ref}(t_j|t_k) = v_{ref}(t_1|t_k), \quad j = 1, 2, \ldots N_p, \tag{10}$$

and

$$\hat{s}_{ref}(t_j|t_k) = \hat{s}_{ref}(t_1|t_k) + T_s \sum_{i=1}^{j-1} \hat{v}_{ref}(t_i|t_k), \ j = 1, \ldots, N_p \tag{11}$$

with $\hat{s}_{ref}(t_1|t_k) = d_0$. The speed forecasting method (10) represents an elementary but widely applicable algorithm (Shakouri and Ordys, 2014) that enables the ACC to

be implemented in real-time for benchmarking purposes. The following terminal cost is used for the ACC:

$$J_{k,\text{ACC}} = W_1 m_f(t_{N_p}|t_k) + W_2 \left(\text{SoC}(t_{N_p}|t_k) - \text{SoC}(0)\right)^2$$
$$+ W_3 \sum_{j=1}^{N_p} \left(\hat{d}(t_j|t_k) - d_{ACC}\right)^2, \quad k = 1, 2 \dots, T/T_s \quad (12)$$

where W_1, W_2, W_3 are constant weights, $\hat{d} = \hat{s}_{ref} - s$ is the anticipated inter-vehicular distance and d_{ACC} is the desired following distance. As such, in addition to the fuel usage and SoC variations (first two terms), the third term in (12) represents a running cost penalizing also the variation in the headway distance.

Within each finite horizon, $J_{k,\text{ACC}}$ is minimized subject to various constraints and boundary conditions (9b)-(9d). More specifically, the dynamic constraints (9b) represent the discretized version of vehicle system (6), with the initial condition $\boldsymbol{x_0}$ for each iteration. $\boldsymbol{x_0}$ is the same as used in the OC case at $t = 0$, and it is updated iteratively based on the system states at $t = t_k$, $k = 1, 2, \dots, T/T_s$. The Ψ inequality constraints (9d) incorporate (1) and (7), which are identical to the OC case.

2.3 Enhanced Adaptive Cruise Control Strategy

The EACC, which is developed in this section, aims to further improve the fuel economy performance of the ACC without losing the real-time control property.

Terminal cost design Similarly to the ACC, the EACC is also formulated as an NMPC problem (9), subject to identical constraints and initial conditions to those of the ACC. However, the terminal cost is redesigned to allow adjustable following distance:

$$J_{k,\text{EACC}} = W_1 m_f(t_{N_p}|t_k) + W_2 \left(\text{SoC}(t_{N_p}|t_k) - \text{SoC}(0)\right)^2$$
$$+ W_3 (\hat{v}_{ref}(t_{N_p}|t_k) - v(t_{N_p}|t_k))^2, \quad k = 1, 2, \dots, T/T_s \quad (13)$$

where the last term penalizes the difference between the terminal speed of both vehicles, as opposed to the ACC that keeps the headway distance fixed. As a consequence, the ego vehicle is able to make use of the inter-vehicular distance variation within an NMPC horizon for fuel economy improvement, while keeping up with the reference speed at the end of the horizon at each iteration. Thus, the terminal cost avoids the sub-optimal solution where the ego vehicle maintains the maximum following distance at the end of the horizon at each iteration that minimizes the ego vehicle travelled distance and hence its fuel usage, regardless of the terminal position and velocity of the reference vehicle.

Reference velocity forecasting In addition to the novel objective function (13), the proposed EACC further incorporates a neural network to provide a more effective reference vehicle velocity prediction, $\hat{v}_{ref}(t_j|t_k)$, $j = 1, 2, \dots N_p$ and associated $\hat{s}_{ref}$ by (11), within each NMPC horizon, as compared to the corresponding constant velocity prediction in the ACC shown in (10).

Neural networks are widely used for time series forecasting as they can be trained to establish a nonlinear mapping relationship between input and output data. For velocity prediction purposes, usually historical velocity sequences are considered as the input of the NN, and the outputs are predicted horizon velocity sequences. Each input-output pattern is composed of a moving window of fixed length, which can be expressed as:

$$[v_{k+1}, v_{k+2}, \dots, v_{k+N_p}] = f_{NN}(v_{k-N_h+1}, \dots, v_{k-1}, v_k),$$

where N_h is the dimension of the input historical velocity sequence, and f_{NN} represents the nonlinear map of the NN predictor, which is obtained by offline training.

In this work, a radial basis function neural network (RBF-NN) is applied for speed forecasting of the EACC. The advantages of the RBF-NN have been examined in (Sun et al., 2014), where the RBF-NN shows better convergence speed and precision in the context of velocity prediction of ground vehicles, as compared to a few other types of network structures. The framework of the RBF-NN is shown in Fig. 4. After the input sequences v_h are received
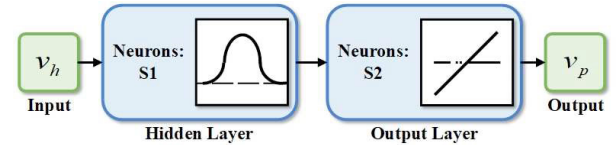

Fig. 4. Scheme of RBF-NN predictor with historical velocity sequences v_h as the input, followed by a Gaussian function-based hidden layer that depicts the nonlinear relationship between input and output, and then the output layer yields the predicted velocity sequences v_p. S_1 and S_2 are the numbers of neurons respectively for the hidden and output layers.

and rearranged, the pre-trained Gaussian function-based hidden layer establish the nonlinear relationship between input and output. Then, the output layer yields output patterns v_p, which are linear combinations of the hidden layer outputs. The number of the neurons in the output layer is identical to the size of output v_p, while that in the hidden layer is tunable and predefined, which determines the precision of the prediction with proper selection of the neuron numbers.

3. NUMERICAL RESULTS

This section provides a comprehensive comparative analysis of the three car following control strategies described in Section 2. All the optimization problems are addressed by the ACADO toolkit, which provides a general framework for efficiently solving optimal control and model predictive control problems based on direct optimal control methods (Ariens et al., 2010). The sampling time of the solver is kept the same for all cases at $T_s = 0.5\,\text{s}$, which provides an appropriate balance between numerical accuracy and computational complexity. Prior to showing the comparative results, a test driving profile of the reference vehicle v_{ref} is introduced next, together with prediction examples of this profile by the RBF-NN.

3.1 Reference Velocity and Prediction

To evaluate the performance of the NMPC methods (ACC and EACC), the urban/suburban cycle JP-15 is selected as the reference velocity, v_{ref}, in this work to emulate a mixed unban/suburban driving environment. Moreover, the training set for the RBF-NN predictor is formed by the four individual components of the WLTP cycle.

Fig. 5 illustrates a prediction example by the RBF-NN utilized in the EACC, for $N_h = 40$ and $N_p = 20$. In other words, it shows 10-second-ahead prediction for the JP-15 cycle based on v_{ref} during the past 20 seconds. As it can be seen, the RBF-NN predictor is able to achieve accurate prediction within a short horizon.

3.2 Comparative Results of the Control Strategies

In order to achieve a fair comparison, all the approaches are tuned to be battery charge sustaining with negligible
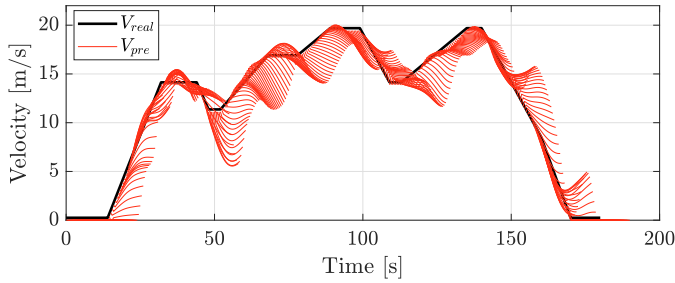
Fig. 5. Reference velocity (JP-15) and the 20-step-ahead ($N_p = 20$) velocity prediction by the RBF-NN driven by the past 40 steps ($N_h = 40$) reference speed data.

differences in the terminal SoC values. Thus, the fuel consumption of each method can be compared without the need to refer to the equivalent fuel, which evaluates the fuel and battery charge consumption under a single paradigm (Shabbir and Evangelou, 2019). The inter-vehicular distance limits are set to avoid both rear-end collision and the disruption of car following scenario. For simplicity, constant limits are employed in this study. Similarly to (Xie et al., 2019), the inter-vehicular distance limits are defined as a linear function of speed, $d_{\min} = b_0 + b_1 v_{\min}$, $d_{\max} = b_0 + b_1 v_{\max}$ where b_0 and b_1 are coefficients, which are set to 5m and 3s, respectively. As the velocity of JP-15 is bounded within $[0, 20]$ m/s, following distance limits are adopted: $d_{\min} = 5$m, $d_{\max} = 65$m. The desired headway distance of the ACC is set to 15m, which is close to the lower distance limit to enable drafting, while leaving enough distance for tolerance to cope with the imprecise speed prediction. The other two methods, OC and EACC, as well as the ACC, are initialized with the same distance value for consistency: $d_0 = d_{ACC} = 15$ m. Moreover, the influence of the prediction horizon is investigated by comparing solutions with different horizon lengths ($N_p = 10$, $N_p = 20$, and $N_p = 30$), to provide further insight into the design of the NMPC-based EACC.

The first case considered is with a prediction horizon for EACC set to $N_p = 10$, which enables accurate velocity forecasts. The optimal ego vehicle speed profile as well as the resulting inter-vehicular distance profile solved by EACC is compared in Fig. 6 with the solutions of OC and ACC with the same horizon length. As it can be seen, both OC and EACC exploit the inter-vehicular distance variation rather than staying closely behind the reference vehicle. This allows OC and EACC to yield smoother speed profiles, and hence lower accelerations, which are expected to be more energy efficient in terms of powertrain operation.

The energy source and other friction energy losses for the whole mission are evaluated for each method, which reinforces some of the earlier observations and conclusions. The histogram in Fig. 7 shows the various power losses for each control strategy. It is clear that the biggest component of losses in all simulated cases corresponds to the PS branch power losses, which is expected since the most inefficient component of the powertrain is the ICE, and the reference vehicle follows a low average-speed profile whereby the air drag losses are not significant. The rolling resistance losses of all three strategies are the same as a fixed distance is travelled in each case. By driving smoothly, OC substantially reduces the energy losses from the PS branch, PL branch and mechanical brakes, and results in the least overall energy losses. Although EACC incurs more PS branch and mechanical braking energy losses than OC, it reduces the aforementioned energy losses as compared to ACC. In addition, ACC also produces more SS branch energy losses as its driving profile (see Fig. 6) demands high power output from both energy
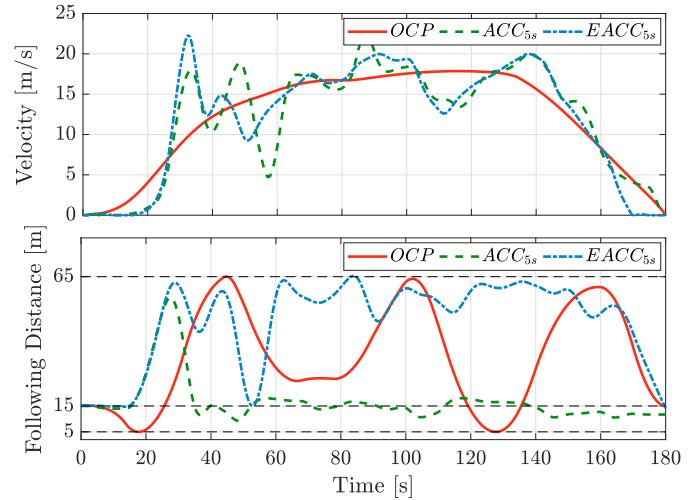

Fig. 6. Optimal ego vehicle driving speeds and the inter-vehicular distances solved by OC, and the two NMPC methods, ACC and EACC with a 10-step (5 s) prediction ahead. The following distance of the ACC has a large overshoot at the beginning due to the transient response to the acceleration of the leading vehicle.
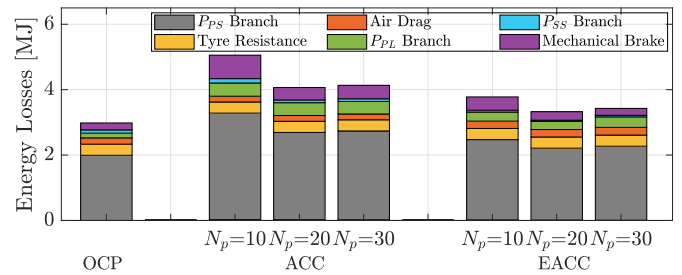

Fig. 7. Energy losses breakdown for the optimal solutions solved by the three strategies (OC, ACC and EACC) for the JP-15 driving cycle as the reference velocity.

sources to perform larger acceleration, and high battery charge rate for larger deceleration. Although ACC is able to cut aerodynamic drag losses by closing the gap between the two vehicles (i.e., drafting), it ends up with the largest overall energy losses because of the more significant losses from the other aspects.

Fig. 8 shows the comparative results of fuel consumption and computation time. The performances of ACC and EACC are compared by using the OC solution as the benchmark. For the prediction horizon of 5 s ($N_p = 10$), the EACC proposed in this work consumes 26.7% more fuel than OC, which is a remarkable improvement as compared to the result of the ACC, which leads to 71.6% more fuel consumption. Both NMPC methods are developed for real-time implementation and thereby they are much more computationally efficient than OC. In comparison with ACC, the additional running time requested by EACC mainly comes from the more advanced speed forecasting approach. The length of the prediction horizon is one of the most crucial factors that influences the performance of NPMC methods. In this context, the horizon length of the ACC and EACC is further increased to $N_p = 20$ and $N_p = 30$ to investigate its impact. As shown in Figs. 7-8, extending the prediction horizon increases the computational burden, but it also enhances the ability to anticipate future behavior of the reference vehicle. Therefore, both the ACC and the EACC benefit from the change of the horizon window from 10 to 20 time steps. However, when N_p is further increased, the optimality of both algorithms starts degrading, since the accuracy of the
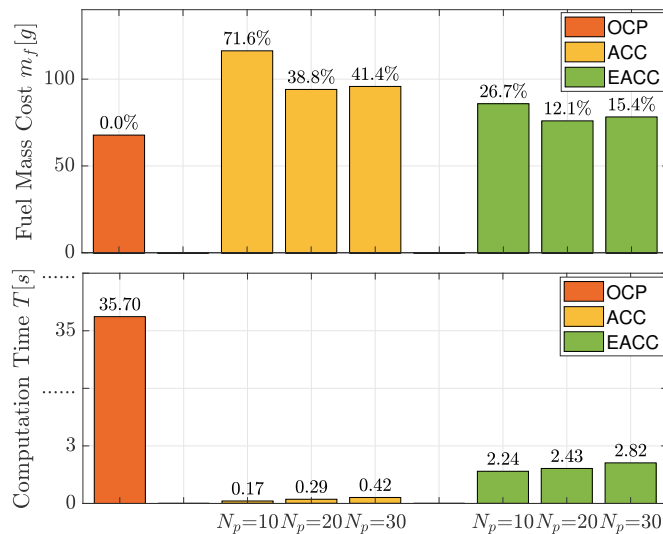
Fig. 8. Fuel consumption and computation time of three control strategies (OC, ACC and EACC). The fuel percentage increase as compared to the OC for each NMPC case is indicated in the top plot.

velocity prediction also drops. The best performing EACC with $N_p = 20$ lags the OC solution by 12.1%. By comparing this EACC case with the best behaved ACC that consumes 38.8% more fuel than the OC, the fuel saved by the EACC is approximately 26%.

4. CONCLUSIONS

This paper proposes the novel control strategy enhanced adaptive cruise control (EACC) for energy management and velocity control of series hybrid electric vehicles in car-following scenarios. This method is developed based on an NMPC framework, in which the velocity of the lead vehicle is predicted by a radial basis function neural network speed forecasting approach. In contrast with the conventional adaptive cruise control (ACC) that aims for a fixed following distance, EACC encourages the ego vehicle to exploit the inter-vehicular distance variation, especially when the vehicle ahead is driven inefficiently. The control performance of the EACC is benchmarked against the full-horizon optimal control (OC) strategy and a suitably designed ACC. The simulation examples based on a typical reference vehicle driving cycle confirm the improvement of EACC over ACC in terms of fuel economy at the expense of the slightly increased computational complexity. Moreover, the fuel economy of the EACC solution is shown to be relatively close to that of the OC solution with a remarkable reduction in the running time.

REFERENCES

Ariens, D., Houska, B., Ferreau, H., and Logist, F. (2010). Acado for matlab user's manual. *Optimization in Engineering Center (OPTEC)*, 1.

Chen, B., Evangelou, S., and Lot, R. (2019). Series hybrid electric vehicle simultaneous energy management and driving speed optimization. *IEEE/ASME Transactions on Mechatronics*, 24(6), 2756 – 2767.

Chen, B., Evangelou, S., and Lot, R. (2018). Fuel efficiency optimization methodologies for series hybrid electric vehicles. In *IEEE Vehicle Power and Propulsion Conference (VPPC)*.

Chen, B. and Evangelou, S.A. (2019). Truncated battery power following strategy for energy management control of series hybrid electric vehicles. In *2019 European Control Conference*. IEEE.

Li, L., Wang, X., and Song, J. (2017a). Fuel consumption optimization for smart hybrid electricvehicle during a car-following process. *Mechanical Systems and Signal Processing*, 87, 17–29.

Li, L., Zhou, L., Yang, C., Xiong, R., You, S., and Han, Z. (2017b). A novel combinatorial optimization algorithm for energy management strategy of plug-in hybrid electric vehicle. *Journal of the Franklin Institute*, 354(15), 6588–6609.

Liu, T., Hu, X., Li, S.E., and Cao, D. (2017). Reinforcement learning optimized look-ahead energy management of a parallel hybrid electric vehicle. *IEEE Transactions on Mechatronics*, 22(4), 1497–1507.

Lujan, J.M., Guardiola, C., Pla, B., and Reig, A. (2018). Analytical optimal solution to the energy management problem in series hybrid electric vehicles. *IEEE Transactions on Vehicular Technology*, 67(8), 6803–6813.

Malikopoulos, A.A., Cassandras, C.G., and Zhang, Y.J. (2018). A decentralized energy-optimal control framework for connected automated vehicles at signal-free intersections. *Automatica*, 93, 244–256.

Martinez, C.M., Hu, X., Cao, D., Velenis, E., Gao, B., and Wellers, M. (2017). Energy management in plug-in hybrid electric vehicles: Recent progress and a connected vehicles perspective. *IEEE Transactions On Vehicular Technology*, 66(6), 4534–4549.

Murphey, Y.L., Park, J., Kiliaris, L., Kuang, M.L., Masrur, M.A., Phillips, A.M., and Wang, Q. (2013). Intelligent hybrid vehicle power control — part ii: Online intelligent energy management. *IEEE Transactions On Vehicular Technology*, 62(1), 69–79.

Rodrigues Lopes, D. and Evangelou, S. (2019). Energy savings from an eco-cooperative adaptive cruise control: a bev platoon investigation. In *2019 European Control Conference (ECC)*. IEEE.

Shabbir, W. and Evangelou, S.A. (2019). Threshold-changing control strategy for series hybrid electric vehicles. *Applied energy*, 235, 761–775.

Shakouri, P. and Ordys, A. (2014). Nonlinear model predictive control approach in design of adaptive cruise control with automated switching to cruise control. *Control Engineering Practice*, 26, 160–177.

Sun, C., Hu, X., Moura, S.J., and Sun, F. (2014). Velocity predictors for predictive energy management in hybrid electric vehicles. *IEEE Transactions on Control Systems Technology*, 23(3), 1197–1204.

Turri, V., Besselink, B., and Johansson, K.H. (2017). Cooperative look-ahead control for fuel-efficient and safe heavy-duty vehicle platooning. *IEEE Transactions on Control Systems Technology*, 25(1), 12–28.

Uebel, S., Murgovski, N., Baker, B., and Sjoberg, J. (2019). A 2-level mpc for energy management including velocity control of hybrid electric vehicle. *IEEE Transactions on Vehicular Technology*.

Xie, S., Hu, X., Liu, T., Qi, S., Lang, K., and Li, H. (2019). Predictive vehicle-following power management for plug-in hybrid electric vehicles. *Energy*, 166, 701–714.

Zhang, F., Hu, X., Langari, R., and Cao, D. (2019). Energy management strategies of connected hevs and phevs: Recent progress and outlook. *Progress in Energy and Combustion Science*, 73, 235–256.

Zhou, W., Zhang, C., Li, J., and Fathy, H.K. (2015). A pseudospectral strategy for optimal power management in series hybrid electric powertrains. *IEEE Transactions on Vehicular Technology*, 65(6), 4813–4825.

Zou, Y., Kong, Z., Liu, T., and Liu, D. (2016). A real-time markov chain driver model for tracked vehicles and its validation: Its adaptability via stochastic dynamic programming. *IEEE Transactions on Vehicular Technology*, 66(5), 3571–3582.